SPACE SCIENCES

10.1126/sciadv.1400050

Refining lunar impact chronology through high spatial resolution $^{40}Ar/^{39}Ar$ dating of impact melts

Cameron M. Mercer,[1]* Kelsey E. Young,[1†] John R. Weirich,[1‡] Kip V. Hodges,[1] Bradley L. Jolliff,[2] Jo-Anne Wartho,[1§] Matthijs C. van Soest[1]

Quantitative constraints on the ages of melt-forming impact events on the Moon are based primarily on isotope geochronology of returned samples. However, interpreting the results of such studies can often be difficult because the provenance region of any sample returned from the lunar surface may have experienced multiple impact events over the course of billions of years of bombardment. We illustrate this problem with new laser microprobe $^{40}Ar/^{39}Ar$ data for two Apollo 17 impact melt breccias. Whereas one sample yields a straightforward result, indicating a single melt-forming event at ca. 3.83 Ga, data from the other sample document multiple impact melt–forming events between ca. 3.81 Ga and at least as young as ca. 3.27 Ga. Notably, published zircon U/Pb data indicate the existence of even older melt products in the same sample. The revelation of multiple impact events through $^{40}Ar/^{39}Ar$ geochronology is likely not to have been possible using standard incremental heating methods alone, demonstrating the complementarity of the laser microprobe technique. Evidence for 3.83 Ga to 3.81 Ga melt components in these samples reinforces emerging interpretations that Apollo 17 impact breccia samples include a significant component of ejecta from the Imbrium basin impact. Collectively, our results underscore the need to quantitatively resolve the ages of different melt generations from multiple samples to improve our current understanding of the lunar impact record, and to establish the absolute ages of important impact structures encountered during future exploration missions in the inner Solar System.

INTRODUCTION

The lunar regolith is a vast archive of geologic samples that collectively record much of the meteorite impact history of the inner Solar System. This repository can be used to quantify the chronology of impact events with high precision and accuracy through isotope geochronology of impact melt products in lunar meteorites and samples returned by the Apollo and Luna missions (*1*–*4*). An important goal of many of these efforts is to constrain the timing of major basin-forming impact events that punctuate lunar history, but such efforts are made more difficult by the complex nature of most samples that contain melt products: impact melt breccias (IMBs). High-resolution imagery of the Moon's surface by NASA's Lunar Reconnaissance Orbiter Camera confirms that even small (ca. 100-m-scale) impact craters on the Moon show visual evidence of melt (*5*), implying that not all IMB melt components can be traced unambiguously to basin-forming impacts. Because the lunar regolith has been reworked over billions of years by continuous meteorite bombardment, we might expect many lunar IMB samples to contain multiple generations of melt, and this hypothesis is supported by evidence for cross-cutting melt veins in many lunar IMB samples (*6*, *7*).

In this contribution, we show how high spatial resolution $^{40}Ar/^{39}Ar$ dating of lunar IMB melt materials in petrographic context using ultraviolet laser ablation microprobe (UVLAMP) technologies can complement more traditional dating methods for unraveling such complexities. New results for Apollo 17 samples 77115 and 73217 confirm that some IMBs (for example, 77115) appear to be monogenetic, whereas others (for example, 73217) contain evidence for multiple impact events spanning several hundred million years. Although the data support the hypothesis that some of the samples collected during the Apollo 17 mission include melts produced by the Imbrium basin-forming impact (*8*–*10*) in addition to those from the Serenitatis basin, IMBs from the Taurus-Littrow regolith also preserve a rich history of more localized impact melting. A comprehensive understanding of the evolution of planetary regoliths will require extensive geochronology campaigns to isolate small, localized impact melting episodes from regional or global (that is, basin-scale) events.

IMBs are complex admixtures of "melt"—glass and neoblastic crystalline aggregates—and "clasts," which are relict crystals (xenocrysts) and lithic fragments (xenoclasts) from the target rocks. This can make it difficult to uniquely interpret the ages of impact events from isotopic dates of impact melt products (*11*–*14*), and poses special challenges for $^{40}Ar/^{39}Ar$ dating (*15*). One concern in particular is that, despite careful sample preparation, relict, incompletely reset clasts may be present in the small chips of IMBs analyzed in conventional incremental heating $^{40}Ar/^{39}Ar$ experiments, which typically mass a few to a few tens of milligrams. Although an impact event can heat target materials to extremely high temperatures, the heterogeneous spatial distribution of peak temperatures and short duration of the thermal pulse is often insufficient to fully reset the Ar isotopic systematics of clasts (*14*, *16*, *17*). Thus, conventional $^{40}Ar/^{39}Ar$ analyses compromised by the presence of clasts may yield anomalously old dates that do not accurately reflect the age of impact [for example, (*18*–*22*)]. In addition, for samples that have experienced multiple impacts on airless bodies like the Moon, it is possible that previous generations of melts may be incorporated

[1]School of Earth and Space Exploration, Arizona State University, Tempe, AZ 85287, USA. [2]Department of Earth and Planetary Sciences and McDonnell Center for the Space Sciences, Washington University, St. Louis, MO 63130, USA.
*Corresponding author: E-mail: cameron.m.mercer@asu.edu
†Present address: Planetary Geodynamics Laboratory, Code 698, NASA Goddard Space Flight Center, Greenbelt, MD 20771, USA.
‡Present address: Centre for Planetary and Space Exploration, Department of Earth Sciences, Western University, London, Ontario N6A 5B7, Canada.
§Present address: GEOMAR Helmholtz Centre for Ocean Research Kiel, Wischhofstr. 1-3, D-24148 Kiel, Germany.

in a newly assembled IMB and have their K-Ar systematics variably affected, ranging from unreset to fully reset depending on the duration and magnitude of the heating they experience. Incremental heating $^{40}Ar/^{39}Ar$ analyses of mixed generations of impact melts and/or partially degassed materials typically yield dates that are difficult to interpret, though evidence for multiple impact events may still be recovered from some samples [for example, (*23*)].

One approach to enable more robust interpretations of $^{40}Ar/^{39}Ar$ data involves dating small masses of material (on the order of micrograms or less) in petrographic context. Some early work using this strategy involved the use of infrared (IR) lasers to heat and melt small sample volumes to explore apparent age variations over spatial scales of a few hundred micrometers (*17*, *24*–*26*). However, IR lasers can cause considerable collateral heating of material adjacent to the area under the laser beam (*27*, *28*), making it difficult to reliably quantify the exact volume of the sample that contributed gas to the analysis. If distinct generations of melt or relict clasts are present within the collateral heating zone, anomalous dates may be obtained. In an effort to avoid this problem, Cohen *et al.* (*29*) successfully used a 100-μm-diameter microcorer to physically extract small aliquots from impact melt clasts in lunar meteorites before $^{40}Ar/^{39}Ar$ dating. By combining petrologic data with their $^{40}Ar/^{39}Ar$ dates, they were able to infer that at least six to nine distinct impact events were represented in the population of melt clasts sampled from only four meteorites. Another alternative, which can sometimes provide even higher spatial resolution, is to use pulsed ultraviolet lasers to ablate, rather than melt, small volumes of a polished sample (*30*). Experimental and theoretical work has shown that ultraviolet lasers with short pulse durations (for example, ≤5 ns) produce very little collateral heating and consequent diffusive loss of helium in apatite (*28*, *31*), implying that the collateral loss of argon (which is significantly less diffusive than helium) is negligible.

Our data for Apollo 17 IMBs were obtained using the UVLAMP method (*30*). Sample 77115 is a "blue-gray," poikilitic, clast-rich IMB that was collected from the Station 7 boulder located at the base of the North Massif during the Apollo 17 mission to the Taurus-Littrow Valley. The Station 7 boulder consists of several distinct lithologies, including a large noritic clast (sample 77215) that is cut by dark veinlets (77075), which are continuous with the blue-gray breccia, and a "green-gray" fragment-laden IMB (77135) that is in contact with the blue-gray lithology (*6*, *32*, *33*). Despite the continuity of the blue-gray breccia and the dark veinlets, Stettler and co-workers (*19*, *20*, *34*) found 77075 to be older than 77115, leading them to suggest that the blue-gray breccia was partially degassed when the younger green-gray breccia (77135) was emplaced. Here, we have focused our attention on thin sections of the blue-gray matrix of 77115. The conventional $^{40}Ar/^{39}Ar$ dates reported in the 1970s (*20*, *34*) for clast-rich and clast-poor fragments of 77115 range from 3.902 ± 0.048 Ga to 3.796 ± 0.039 Ga (table S1) when they are recalculated using modern values for ^{40}K decay parameters and the irradiation monitor age (see Supplementary Materials and Methods). (Throughout this paper, all dates are reported at the 2σ, ca. 95% confidence level unless otherwise noted.)

Sample 73217 is a polymict impact melt rock that was collected at Station 3 from the rim of a small crater in the landslide material from the South Massif (*35*). Petrologic studies of a variety of fragments from this sample have identified multiple distinct breccia types (with generally aphanitic and partly glassy matrices) that have been interpreted to record a prolonged and complex history of crystallization, brecciation, and impact [for example, (*36*–*38*)]. A combined zircon U/Pb date of $4.356^{+0.023}_{-0.014}$ Ga was interpreted by Compston *et al.* (*39*) to be the crystallization age of a gabbronorite clast, and they observed slight Pb loss for some zircon grains that they attributed to one or more thermal events as young as 1.1 Ga. Ion microprobe U/Pb dates for apatite, merrillite, and three distinct morphological types of zircon from a different section of this sample were interpreted by Grange *et al.* (*2*) to represent two impact events at 4.335 ± 0.005 Ga and 3.934 ± 0.012 Ga (ca. 95% confidence level).

RESULTS

Backscattered electron (BSE) image mosaics of the ca. 100-μm-thick sections that we studied (77115,121 and 73217,83) are shown in Fig. 1, along with x-ray elemental maps of thin section 73217,84, which was prepared as a facing section to 73217,83. The section 77115,121 is a vuggy IMB with a very fine-grained crystalline matrix consisting largely of neoblastic plagioclase and pyroxene in a micropoikilitic texture, with scattered olivine grains and ilmenite throughout. This matrix contains abundant xenoclasts of anorthosite, norite, and dunite and xenocrysts of their mineral constituents that are up to ca. 3 mm in size (Fig. 1A). In contrast, sections 73217,83 and 73217,84 contain three distinct breccia domains (Fig. 1, B to D): (1a) a medium-grained noritic anorthosite assemblage with plagioclase grains up to millimeters in size and orthopyroxene grains up to ca. 750 μm in size; (1b) a fine-grained brecciated equivalent of domain 1a; (2) a clast-rich, quartz-clast bearing gabbronoritic melt breccia with a potassic, glassy matrix and a phosphate-rich composition that is more ferroan than domain 1; and (3) a very fine-grained, clast-poor crystalline noritic melt breccia containing abundant plagioclase and low-Ca pyroxene. Domain 3 also has a potassic matrix, but it is generally less concentrated than those of domains 1b and 2. Both domains 2 and 3 appear to be quartz-normative. Detailed petrography of the boundaries between domain 2 and other domains suggests chemical mobility across the boundaries. For example, domain 1b near the boundary is enriched in potassium, and the enrichment zone in places appears to extend into domain 3 (Fig. 1D). The elevated potassium content of the melt materials in domains 1 to 3 is unusual for Apollo 17 impact melts, implying target materials that are distinct from those of other impact-melted targets for samples collected in the Taurus-Littrow Valley.

We used the UVLAMP system to target 15 small melt volumes and 11 monomineralic and lithic clasts for $^{40}Ar/^{39}Ar$ dating in 77115,121 (Fig. 1A, fig. S1, and table S2). Although the analytical uncertainties of individual dates are relatively large as a consequence of the small material volumes ablated, the population of melt dates constitute a single major mode on a probability density plot (PDP; Fig. 2A). When plotted on an isotope correlation diagram (Fig. 2B), these 15 melt analyses form an isochron with a date of 3.834 ± 0.020 Ga [mean squared weighted deviation (MSWD) = 1.01]. Analyses of clasts in 77115,121 yielded considerably older dates, ranging from 4.23 ± 0.25 Ga to 3.892 ± 0.067 Ga (table S2). Note that a few of the melt dates have probability density distributions that overlap those of the clast population, potentially indicating that the ablation volumes may have been contaminated by small amounts of clast material that was undetected during the targeting process (see Supplementary Materials and Methods). However, given the value of the MSWD for the isochron (1.01) and because there are no clear visual indications for clast contamination from an inspection of the laser pits under a microscope,

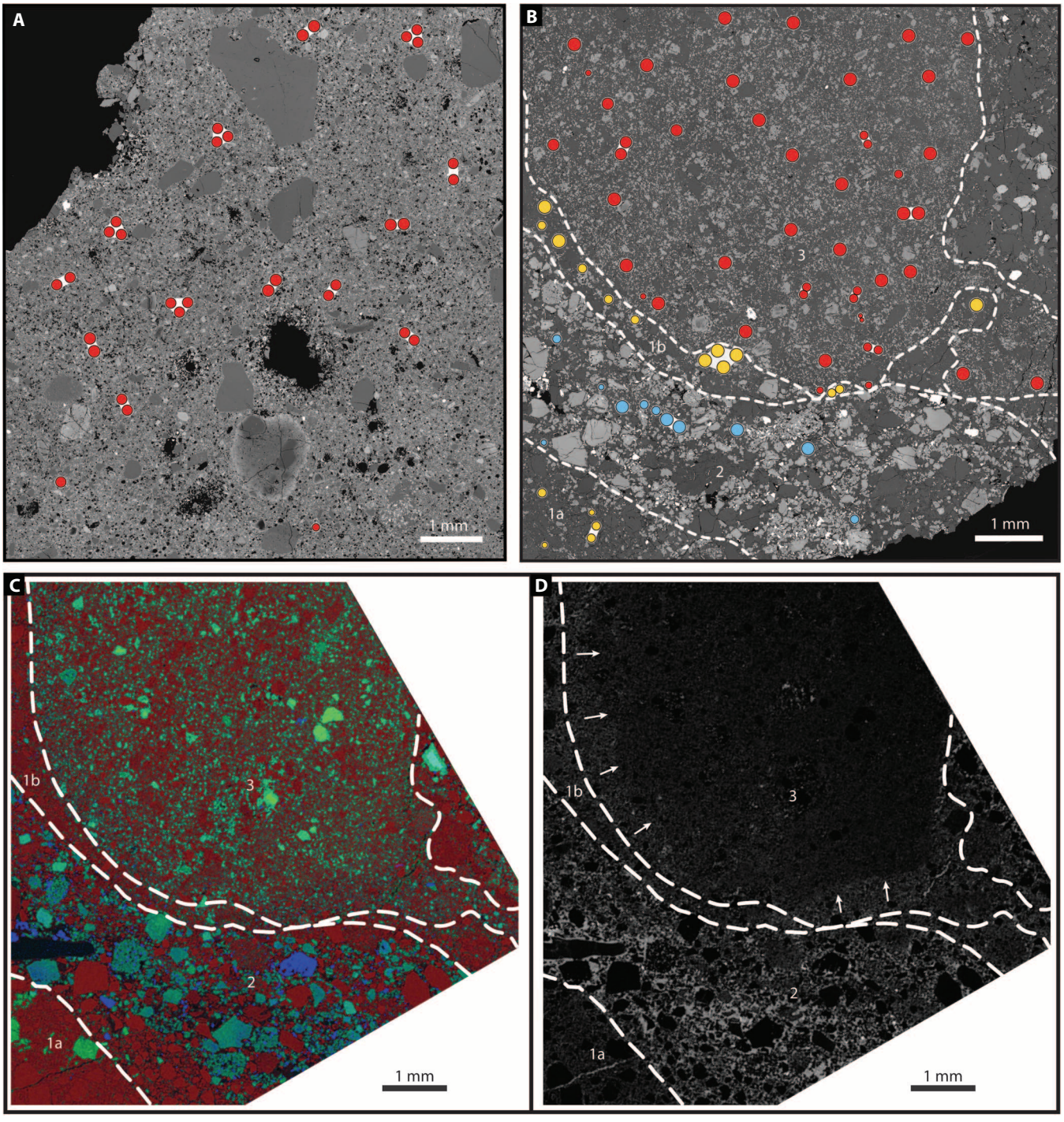

Fig. 1. BSE image mosaics and x-ray elemental maps of the studied sections of 77115 and 73217. White dashed lines mark the lithologic boundaries of domains 1, 2, and 3 in the sections of 73217 (B to D). (**A**) BSE mosaic of 77115,121 with the locations and dimensions of UVLAMP melt analyses shown as red circles. (**B**) BSE mosaic of 73217,83 with the locations and dimensions of UVLAMP melt analyses in domains 1 (yellow), 2 (blue), and 3 (red). The coarse-grained region in the upper right is a gabbroic granulite. (**C**) Combined x-ray elemental map of Al-Mg-Fe (R-G-B) in 73217,84 (the thin section facing 73217,83). Plagioclase grains are generally red, pyroxenes and olivines are green, and ilmenite is blue; the black elongate grain in domain 2 is quartz. (**D**) X-ray elemental map of K in 73217,84; arrows denote the apparent enrichment of K in domain 3. See the text for descriptions of domains labeled 1a, 1b, 2, and 3 in (B) to (D). Scale bars, 1 mm.

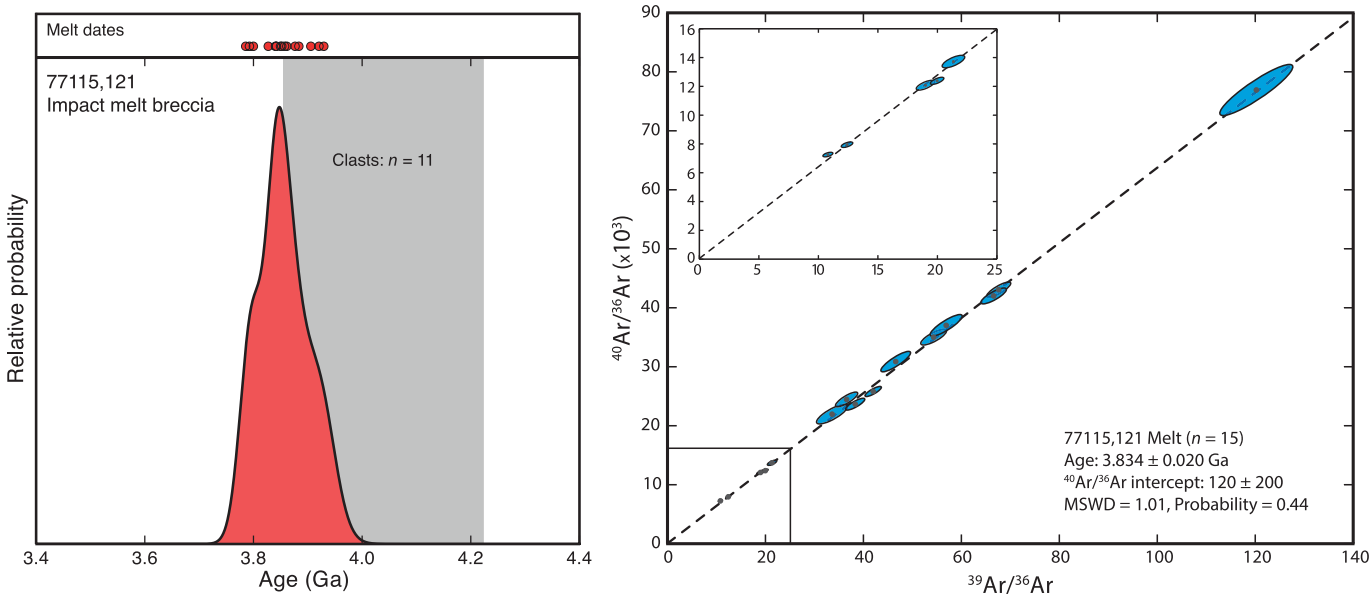

Fig. 2. UVLAMP $^{40}Ar/^{39}Ar$ results for 77115,121. (**A**) Summed PDP of melt dates (red) with individual dates depicted as small red circles above. The gray region represents the range of dates obtained for clasts in 77115,121. (**B**) Isotope correlation plot of $^{40}Ar/^{36}Ar$ versus $^{39}Ar/^{36}Ar$ and linear regression (dashed line) for melt analyses in 77115,121. The inset figure is an enlarged plot of the boxed region near the origin. The data have been corrected for the presence of nucleogenic and cosmogenic isotopes (see Materials and Methods for details). Error ellipses and uncertainties are all 2σ.

there is no strong statistical or observational basis for identifying and rejecting potential outliers in the regression.

During UVLAMP analyses of 73217,83, we targeted 13 melt volumes in domain 1, 10 melt volumes in domain 2, 40 melt volumes in domain 3, and 8 clasts within domains 2 and 3 (Fig. 1B, fig. S2, and table S3). Represented on a PDP, the populations of $^{40}Ar/^{39}Ar$ dates from the three domains and clasts are distinct and span a range from ca. 4.0 to 3.2 Ga (Fig. 3A). One population of clast dates range from 3.788 ± 0.088 Ga to 3.721 ± 0.052 Ga, whereas a second group of clast dates range from 3.973 ± 0.019 Ga to 3.902 ± 0.030 Ga. Both sets of clasts are older than the melt matrixes of their host breccia domains (fig. S2 and table S3). All 13 melt analyses from domain 1 form an isochron with a date of 3.808 ± 0.013 Ga (MSWD = 0.86; Fig. 3B). Note that the PDP for domain 1 has a minor mode that overlaps the younger population of clast dates and a minor mode in the PDP of domain 3 dates (Fig. 3A). Although this minor mode in domain 1 may represent some analyses that incorporated mixed materials, we found no visual evidence for this during our inspection of the ablation pits (see Supplementary Materials and Methods). Also, because the MSWD is near unity, we find no statistical basis for identifying and rejecting potential outliers in the regression.

Regressing all 10 analyses from domain 2 yields a date of 3.644 ± 0.020 Ga with a relatively poor MSWD of 2.07 ($P = 0.036$). Because the MSWD is larger than expected for a linear regression of $n = 10$ points (see Supplementary Materials and Methods), we could expand the uncertainty by $\sqrt{\text{MSWD}}$ to obtain a conservative uncertainty of 0.028 Ga (*40*). This commonly used approach to handling geochronologic data sets with excess dispersion assumes that all analyzed pit volumes have been in isotopic equilibrium since the domain 2 melting event, and that the relatively poor MSWD simply reflects an underestimation of the analytical imprecision of the analyses. We also explored an alternative approach that used the Hampel identifier with a conservative threshold value of 6 to select potential outliers for rejection from the regression (*41*) (see Statistical analysis of Supplementary Materials and Methods for details). This approach identified a single outlier (analysis 652-04), which represents the youngest date from domain 2 (table S3). Inasmuch as the material analyzed for 652-04 may have experienced some ^{40}Ar loss due to a later thermal event or events (see below), we could omit this analysis from the domain 2 regression exercise to obtain an isochron date of 3.664 ± 0.021 Ga and a good MSWD of 0.88 (Fig. 3C). Note that the $\sqrt{\text{MSWD}}$ error expansion technique and the Hampel outlier identifier approach yield statistically indistinguishable age estimates for the primary domain 2 melting event, but we regard the 3.664 ± 0.021 Ga estimate as more likely correct in this instance.

The population of $^{40}Ar/^{39}Ar$ dates for domain 3 is complex, with at least five distinct modes of apparent ages spanning a period of several hundred million years (Fig. 3A). The oldest minor mode in the domain 3 PDP is defined by three sample volumes with model dates that overlap the younger population of clast dates for the sample as well as a minor mode in the PDP of domain 1 dates. This most likely represents contamination of these melt volumes by older clasts or domain 1 melt that was encountered at depth during laser ablation but was not observed in microscopic examination of the 73217,83 section. The highest-frequency mode for the domain (labeled 3A in Fig. 3A) is at 3.609 ± 0.012 Ga based on the error-weighted mean of 13 analyses with individual dates that overlap the peak within 3σ (see Statistical analysis of Supplementary Materials and Methods for details). Similarly, the youngest mode (labeled 3B in Fig. 3A) has an error-weighted date of 3.281 ± 0.023 Ga based on five analyses that overlap the peak within 3σ. (The analyses selected from modes 3A and 3B are specified in table S3, and their locations are designated in fig. S2.) However, these estimates are based on the individual dates that contribute to modes 3A and 3B where we have assumed a value of $^{40}Ar/^{36}Ar = 1 \pm 1$ (1σ) for "trapped" lunar argon. One advantage of calculating isochron dates is that a $^{40}Ar/^{36}Ar$ value does not need to be assumed (note that all of the isochron regressions for 77115,121 and 73217,83 yielded $^{40}Ar/^{36}Ar$

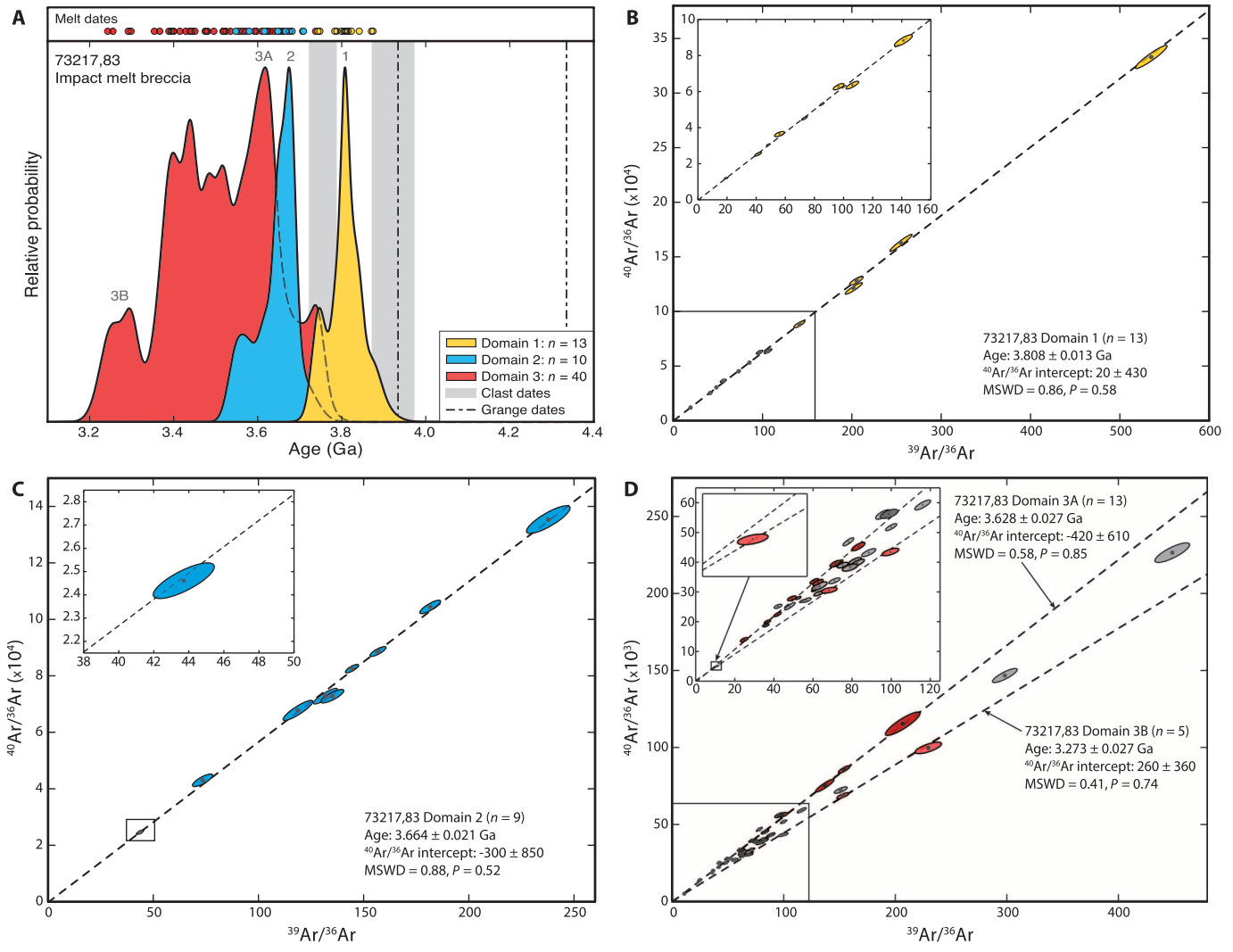

Fig. 3. UVLAMP $^{40}Ar/^{39}Ar$ results for 73217,83. (**A**) Summed PDP of the dates for the three melt domains with individual dates depicted as small colored circles above (yellow, domain 1; blue, domain 2; red, domain 3). Vertical gray bars indicate ranges of two populations of clast dates from 73217,83. The vertical dashed lines indicate U/Pb dates for zircons and phosphates from another section of 73217 interpreted by Grange *et al.* (*2*) to represent impact melting events. (**B** to **D**) Isotope correlation plots of $^{40}Ar/^{36}Ar$ versus $^{39}Ar/^{36}Ar$ with linear regressions shown as dashed lines. Inset figures are enlarged plots of the boxed regions in their parent figures. The data have been corrected for the presence of nucleogenic and cosmogenic isotopes (see Materials and Methods for details). Error ellipses and uncertainties are all 2σ. (B) Isotope correlation plot for analyses in domain 1. (C) Isotope correlation plot of domain 2 analyses. Note: The one analysis that was rejected as an outlier is not shown (see the text for details). It would plot below the regressed line, up and to the right outside of the present bounds. (D) Isotope correlation plot of domain 3 data. Points shown as dark red ellipses were selected from mode 3A of the PDP (see the text for details) and regressed (upper line) to constrain the upper bound of the range of apparent ages measured for domain 3. Points shown as light red ellipses were selected from mode 3B of the PDP and regressed (lower line) to constrain the lower bound of the range of apparent ages for domain 3. The locations of the analyses that constitute modes 3A and 3B are shown in fig. S2. All other data are shown as unfilled ellipses.

intercepts that are statistically indistinguishable from the value 1 ± 1; Figs. 2 and 3). We therefore used the same analyses that were selected for the above estimates based on their overlapping the peaks of modes 3A and 3B, and regressed them to determine isochron dates (Fig. 3D). Note that the selected points and regressed lines bracket the complete set of domain 3 data in the isotope correlation diagram except for the three analyses that lie above the regression line for 3A. These three points correspond to the analyses in the oldest minor mode in the PDP, which we suspect may have been contaminated by the incorporation of older materials. The bracketing isochrons yield dates of 3.628 ± 0.027 Ga for mode 3A (MSWD = 0.58) and 3.273 ± 0.027 Ga for mode 3B (MSWD = 0.41). These are our preferred estimates for the dates bracketing the observed range of apparent ages in domain 3 exclusive of the three potentially contaminated analyses.

DISCUSSION

Sample 77115 is a good example of an IMB with a relatively simple history. From petrographic observations, the crystalline matrix appears

to represent a single generation of impact melt. This interpretation is supported by the isotopic data because the UVLAMP $^{40}Ar/^{39}Ar$ dates form a single population, and so we interpret the 3.834 ± 0.020 Ga isochron date to represent the age of the impact event responsible for all of the melt analyzed in this subsample of 77115. This date is statistically indistinguishable from two of the three dates reported by Stettler *et al.* (*20*, *34*) for the blue-gray matrix of 77115 (table S1). The older dates (ranging from 4.23 ± 0.25 Ga to 3.892 ± 0.067 Ga) for the clasts in 77115,121 likely reflect varying degrees of partial resetting rather than the timing of primary crystallization.

Petrologic observations of our sections of 73217 indicate three distinct melt breccia domains based on differences in modal mineralogy, grain size, and geochemistry (Fig. 1, B to D). However, the textural relationships between the different domains do not provide direct constraints on their relative ages. For example, x-ray elemental maps of the thin section 73217,84 show evidence of potassium enrichment in domains 1b and 3 near domain 2 (Fig. 1D), which could reasonably be interpreted as an indication that K-rich domain 2 is younger, and might be the youngest melt in 73217,83. In light of the UVLAMP data, we prefer an alternative explanation: that the K-enrichment in domain 1 is indeed related to the injection of K-rich domain 2 melt, but that the marginal K-enrichment of domain 3 melt reflects partial assimilation of portions of domain 2 and the intervening selvage of domain 1b. This insight underscores the value of integrating petrographic and geochronologic work when establishing the geologic history of complex breccias.

Using our petrographic observations, we grouped the UVLAMP $^{40}Ar/^{39}Ar$ dates into separate populations corresponding to the three different breccia domains. We interpret the 3.808 ± 0.013 Ga isochron date as the probable age of the impact that generated domain 1 melt. Similarly, we take the isochron date of 3.664 ± 0.021 Ga (determined after rejecting analysis 652-04 as a probable outlier) as the best estimate for the age of the melting event that formed the domain 2 breccia. The data for domain 3 cannot be interpreted uniquely. In one viable scenario, the analyses that constitute mode 3A in the PDP (Fig. 3A) could represent an impact event that initially formed the domain 3 melt at 3.628 ± 0.027 Ga, and mode 3B could represent a second impact event at 3.273 ± 0.027 Ga (see fig. S2 for the locations of analyses that constitute modes 3A and 3B). Alternatively, whereas mode 3A may reflect the time of initial domain 3 melting, mode 3B may represent a later thermal event (likely due to an impact) that preferentially degassed some regions of domain 3 and presumably some regions of domains 1 and 2. In this case, the mode 3B date must be viewed as a maximum age for the thermal event. A third possible scenario derives from the observation that the probable age of domain 2 melt (3.664 ± 0.021 Ga) marginally overlaps the date for mode 3A (3.628 ± 0.027). It is plausible that the domain 3 melt was formed penecontemporaneously with domain 2 melt, but was more susceptible to partial degassing by a later thermal event (with a maximum age indicated by mode 3B). This possibility is not unreasonable because the matrix of domain 3 is generally slightly more fine-grained than that of domain 2. Whichever of these alternative interpretations are correct, the UVLAMP data from a single 8.5 mm × 9 mm section of 73217 record evidence for at least three distinct impact events: one at ca. 3.81 Ga that formed the domain 1 melt, a second at ca. 3.66 Ga that formed the domain 2 melt (and possibly the domain 3 melt), and a third that is ≤3.27 Ga.

Most published $^{40}Ar/^{39}Ar$ dates for lunar materials were obtained through incremental heating studies of melt breccia samples large enough to be aggregates of melts and preimpact clasts. With its high spatial resolution, the UVLAMP $^{40}Ar/^{39}Ar$ method offers an important complementary way to date impact melts that is especially useful for polygenetic IMBs. Our limited data set confirms that the impact histories of lunar IMBs are very complex, even on the scale of a single 8.5 mm × 9 mm thin section, making it challenging to determine the ages of major basin-forming events unambiguously from these materials. A reasonable tactic for interpreting complex data sets is that the oldest direct dates for abundant melt components—ca. 3.83 Ga to 3.81 Ga for the two samples discussed here—represent the major impact melt–forming event in the samples' source area, whereas younger dates likely represent subsequent, localized impacts. [We interpret the rare, older impact melt minerals studied by Grange *et al.* (*2*) in 73217 to be xenocrysts that survived the impact event responsible for the primary melt in 73217 without having their Pb isotopic systematics compromised.] We suspect that many more dates will be required to better refine the ages of the melt-forming events in the source region (or regions) of the Apollo 17 sample archive, particularly for texturally complex, polygenetic IMBs, but the initial data presented here provide some important insights.

Lunar Reconnaissance Orbiter Camera images of the Sculptured Hills of the Taurus Highlands suggest that the source regions of samples returned from the Apollo 17 mission may be dominated by Imbrium basin ejecta rather than Serenitatis basin ejecta (*10*), a hypothesis that was suggested by some early workers based on the distributions of impact melt dates for IMBs collected at the Apollo 14, 16, and 17 landing sites [for example, (*8*)] and on the basis of basin ejecta theory and modeling [for example, (*9*)]. A ca. 3.83 to 3.81 Ga age for primary melt solidification in samples 77115,121 and 73217,83, broadly consistent with several previous estimates of the age of the Imbrium basin [for example, (*42*–*44*)], would support this hypothesis, although we acknowledge that others [for example, (*45*, *46*)] have suggested both somewhat younger and somewhat older ages for the Imbrium event. Published estimates for the age of the Serenitatis basin [for example, (*1*, *2*, *47*)] are uniformly older than the oldest major melt components analyzed here. Note that our results do not necessarily preclude the interpretation by Grange *et al.* (*2*) that one group of zircons and phosphates found in 73217 crystallized from melts produced by the Serenitatis basin-forming impact at ca. 3.93 Ga. Because the Imbrium basin impinges upon the rim of Serenitatis, it is plausible that melt products originally present in the Serenitatis ejecta sheet were later incorporated as components in breccias assembled during the Imbrium basin-forming event. Finally, the apparent age of the youngest impact event recorded by 73217,83 (≤3.27 Ga) is interesting in light of the finding of Shuster *et al.* (*3*) that a significant ca. 3.3 Ga impact event affected the Apollo 16 landing site, perhaps indicating a regionally significant impact flux at that time.

Recently, Sharp *et al.* (*48*) reported highly siderophile element (HSE) analyses for a variety of poikilitic and aphanitic Apollo 17 impact melts and interpreted similarities in HSE concentrations to imply that either a single impactor was responsible for all Apollo 17 impact melts or multiple impactors contributed to a single dominant HSE signature in the melts. Although we did not analyze the same samples for which HSE abundances were reported, our data and those of Grange *et al.* (*2*) support the second hypothesis rather than the first, consistent with the fact that the HSE signature identified by Sharp *et al.* is different from that of any of the known meteorite groups.

Evidence for marked inter- and intrasample variability in the preserved impact record of the Moon has important implications for the design of sampling and sample analysis strategies for materials returned from future human and robotic exploration missions in the inner Solar System. If a few small samples must be returned from exploration targets, breccia samples with visual evidence of a polygenetic origin (such as 73217) should be regarded as high-value opportunities. Through the application of multiple chronometers, using a methodology that integrates bulk and microanalytical procedures such as UVLAMP, individual polygenetic breccias may yield remarkable insights into the complex impact history of planetary regoliths.

MATERIALS AND METHODS

Polished ca. 100-μm-thick ("thick") sections and corresponding polished ca. 32-μm-thick ("thin") sections were prepared for each of the samples 77115 and 73217 using special procedures at NASA Johnson Space Center in that they were mounted in cyanoacrylate rather than organic epoxy for polishing. This change was necessary to prevent the introduction of organic compounds into the mass spectrometer during $^{40}Ar/^{39}Ar$ analysis. BSE images were obtained for all sections using the JEOL JXA-8200 electron microprobe at Washington University in St. Louis operated with a 15-kV accelerating potential and a 10-nA beam current, and x-ray element maps were made of the thin sections to aid in planning UVLAMP analytical campaigns for the corresponding thick sections. Small portions (ca. 9 × 9 mm) of the thick sections were shielded in cadmium and irradiated for ca. 203 hours in the medium-flux positions at the McMaster University reactor in Hamilton, Canada, along with the age monitor PP20 (1078.9 ± 4.6 Ma, 1σ; see Supplementary Materials and Methods for additional details), and CaF_2 salts and kalsilite glass to determine interfering nuclear production ratios.

Laser microprobe $^{40}Ar/^{39}Ar$ analyses were conducted at Arizona State University using a NewWave Research UP193X ultraviolet (193 nm) ArF pulsed laser to create 70- to 200-μm-diameter near-cylindrical pits with typical depths between 16 and 38 μm. The extracted gas was purified and equilibrated into a high-sensitivity multicollector mass spectrometer (Noblesse, Nu Instruments) equipped with a Nier-type source and zoom optics to measure argon isotopes. Measurements were corrected for detector baselines, bracketing measurement blanks, instrument mass discrimination, interfering "nucleogenic" isotopes produced during irradiation, the decay of ^{39}Ar and ^{37}Ar after irradiation, and cosmogenic isotope production in the lunar environment. Summaries of our laser microprobe $^{40}Ar/^{39}Ar$ data are available in tables S2 and S3.

Model dates were calculated for individual analyses assuming a value of $^{40}Ar/^{36}Ar = 1 \pm 1$ (1σ) for trapped lunar argon and represented on PDPs (Figs. 2A and 3A). The $^{40}Ar/^{39}Ar$ data for distinct melt breccia domains from each sample were also plotted on isotope correlation, or "isochron," diagrams with axes of $^{40}Ar/^{36}Ar$ versus $^{39}Ar/^{36}Ar$ (after correction for the presence of nucleogenic and cosmogenic isotopes). Linear regression analyses of these data were performed using the method of York *et al.* (*40*). The goodness of fit of the regressions was evaluated using the MSWD of the data about the best-fit line (*49*). See Supplementary Materials and Methods for additional details.

SUPPLEMENTARY MATERIALS

Supplementary materials for this article is available at http://advances.sciencemag.org
Materials and Methods
Fig. S1. BSE image mosaic of 77115,121,1 with UVLAMP analysis locations.
Fig. S2. BSE image mosaic of 73217,83,1 with UVLAMP analysis locations.
Table S1. Recalculated literature data.
Table S2. UVLAMP $^{40}Ar/^{39}Ar$ data for 77115,121,1.
Table S3. UVLAMP $^{40}Ar/^{39}Ar$ data for 73217,83,1.
Table S4. Irradiation history for 77115,121 and 73217,83, PP20 age monitor, and flux monitors.
References (*50*–*62*)

REFERENCES AND NOTES

1. D. Stöffler, G. Ryder, B. A. Ivanov, N. A. Artemieva, M. J. Cintala, R. A. F. Grieve, Cratering history and lunar chronology. *Rev. Mineral. Geochem.* **60**, 519–596 (2006).
2. M. L. Grange, A. A. Nemchin, R. T. Pidgeon, N. Timms, J. R. Muhling, A. K. Kennedy, Thermal history recorded by the Apollo 17 impact melt breccia 73217. *Geochim. Cosmochim. Acta* **73**, 3093–3107 (2009).
3. D. L. Shuster, G. Balco, W. S. Cassata, V. A. Fernandes, I. Garrick-Bethell, B. P. Weiss, A record of impacts preserved in the lunar regolith. *Earth Planet. Sci. Lett.* **290**, 155–165 (2010).
4. V. A. Fernandes, J. Fritz, B. P. Weiss, I. Garrick-Bethell, D. L. Shuster, The bombardment history of the Moon as recorded by ^{40}Ar-^{39}Ar chronology. *Meteorit. Planet. Sci.* **48**, 241–269 (2013).
5. J. B. Plescia, M. J. Cintala, Impact melt in small lunar highland craters. *J. Geophys. Res.* **117** (2012).
6. H. H. Schmitt, Apollo 17 report on the Valley of Taurus-Littrow: A geological investigation of the valley visited on the last Apollo mission to the Moon. *Science* **182**, 681–690 (1973).
7. D. Stöffler, H.-D. Knöll, U. Maerz, Terrestrial and lunar impact breccias and the classification of lunar highland rocks. *Proc. Lunar Planet. Sci. Conf.* **10**, 639–675 (1979).
8. G. A. Schaeffer, O. A. Schaeffer, ^{39}Ar-^{40}Ar ages of lunar rocks. *Proc. Lunar Planet. Sci. Conf.* **8**, 2253–2300 (1977).
9. L. A. Haskin, R. L. Korotev, K. M. Rockow, B. L. Jolliff, The case for an Imbrium origin of the Apollo thorium-rich impact-melt breccias. *Meteorit. Planet. Sci.* **33**, 959–975 (1998).
10. P. D. Spudis, D. E. Wilhelms, M. S. Robinson, The Sculptured Hills of the Taurus Highlands: Implications for the relative age of Serenitatis, basin chronologies and the cratering history of the Moon. *J. Geophys. Res.* **116** (2011).
11. A. Deutsch, U. Schärer, Dating terrestrial impact events. *Meteorit. Planet. Sci.* **29**, 301–322 (1994).
12. D. D. Bogard, Impact ages of meteorites: A synthesis. *Meteorit. Planet. Sci.* **30**, 244–268 (1995).
13. F. Jourdan, W. U. Reimold, A. Deutsch, Dating terrestrial impact structures. *Elements* **8**, 49–53 (2012).
14. K. E. Young, M. C. van Soest, K. V. Hodges, E. B. Watson, B. A. Adams, P. Lee, Impact thermochronology and the age of Haughton impact structure, Canada. *Geophys. Res. Lett.* **40**, 3836–3840 (2013).
15. F. Jourdan, The $^{40}Ar/^{39}Ar$ dating technique applied to planetary sciences and terrestrial impacts. *Aust. J. Earth Sci.* **59**, 199–224 (2012).
16. E. K. Jessberger, T. Kirsten, T. Staudacher, One rock and many ages—Further K-Ar data on consortium breccia 73215. *Proc. Lunar Planet. Sci. Conf.* **8**, 2567–2580 (1977).
17. G. Eichhorn, J. J. McGee, O. B. James, O. A. Schaeffer, Consortium breccia 73255: Laser ^{39}Ar-^{40}Ar dating of aphanite samples. *Proc. Lunar Planet. Sci. Conf.* **10**, 763–788 (1979).
18. E. K. Jessberger, J. C. Huneke, F. A. Podosek, G. J. Wasserburg, High resolution argon analysis of neutron-irradiated Apollo 16 rocks and separated minerals. *Lunar Sci. Conf.* **5**, 1419 (1974).
19. A. Stettler, P. Eberhardt, J. Geiss, N. Grogler, ^{39}Ar-^{40}Ar ages of samples from the Apollo 17 station 7 boulder and implications for its formation. *Earth Planet. Sci. Lett.* **23**, 453–461 (1974).
20. A. Stettler, P. Eberhardt, J. Geiss, N. Grogler, S. Guggisberg, Age sequence in the Apollo 17 Station 7 boulder. *Proc. Lunar Planet. Sci. Conf.* **6**, 771–773 (1975).
21. G. Turner, P. H. Cadogan, The history of lunar bombardment inferred from ^{40}Ar-^{39}Ar dating of highland rocks. *Proc. Lunar Planet. Sci. Conf.* **6**, 1509–1538 (1975).
22. P. Maurer, P. Eberhardt, J. Geiss, N. Grogler, A. Stettler, G. M. Brown, A. Peckett, U. Krahenbuhl, Pre-Imbrian craters and basins: Ages, compositions and excavation depths of Apollo 16 breccias. *Geochim. Cosmochim. Acta* **42**, 1687–1720 (1978).
23. S. Wang, I. McDougall, N. Tetley, T. M. Harrison, $^{40}Ar/^{39}Ar$ age and thermal history of the Kirin chondrite. *Earth and Planet. Sci. Lett.* **49**, 117–131 (1980).
24. T. Plieninger, O. A. Schaeffer, Laser probe ^{39}Ar-^{40}Ar ages of individual mineral grains in lunar basalt 15607 and lunar breccia 15465. *Proc. Lunar Planet. Sci. Conf.* **7**, 2055–2066 (1976).
25. H. W. Müller, T. Plieninger, O. B. James, O. A. Schaeffer, Laser probe ^{39}Ar-^{40}Ar dating of materials from consortium breccia 73215. *Proc. Lunar Planet. Sci. Conf.* **8**, 2551–2565 (1977).

26. G. Eichhorn, O. B. James, O. A. Schaeffer, H. W. Müller, Laser ^{39}Ar-^{40}Ar dating of two clasts from consortium breccia 73215. *Proc. Lunar Planet. Sci. Conf.* **9**, 855–876 (1978).
27. W. E. Hames, K. V. Hodges, Laser ^{40}Ar/^{39}Ar evaluation of slow cooling and episodic loss of ^{40}Ar from a sample of polymetamorphic muscovite. *Science* **261**, 1721–1723 (1993).
28. S. P. Kelley, D. J. Cherniak, K. A. Farley, J. Schwanethal, Testing the limits to high spatial resolution laser analysis of noble gases in natural and experimental samples. *Geochim. Cosmochim. Acta* **73**, A636 (2009).
29. B. A. Cohen, T. D. Swindle, D. A. Kring, Geochemistry and ^{40}Ar-^{39}Ar geochronology of impact-melt clasts in feldspathic lunar meteorites: Implications for lunar bombardment history. *Meteorit. Planet. Sci.* **40**, 755–777 (2005).
30. S. P. Kelley, N. O. Arnaud, S. P. Turner, High spatial resolution ^{40}Ar/^{39}Ar investigations using an ultra-violet laser probe extraction technique. *Geochim. Cosmochim. Acta* **58**, 3519–3525 (1994).
31. M. C. van Soest, B. D. Monteleone, K. V. Hodges, J. W. Boyce, Laser depth profiling studies of helium diffusion in Durango fluorapatite. *Geochim. Cosmochim. Acta* **75**, 2409–2419 (2011).
32. W. R. Muehlberger, R. M. Batson, E. A. Cernan, V. L. Freeman, M. H. Hait, H. E. Holt, K. A. Howard, E. D. Jackson, K. B. Larson, V. S. Reed, J. J. Rennilson, H. H. Schmitt, D. H. Scott, R. L. Sutton, D. Stuart-Alexander, G. A. Swann, N. J. Trask, G. E. Ulrich, H. G. Wilshire, E. W. Wolfe, *Preliminary Geologic Investigation of the Apollo 17 Landing Site* (NASA, Washington, DC, 1973), pp. 6-1–6-91.
33. S. R. Winzer, D. F. Nava, S. Schuhmann, C. W. Kouns, R. K. L. Lum, J. A. Philpotts, Major, minor and trace element abundances in samples from the Apollo 17 station 7 boulder: Implications for the origin of early lunar crustal rocks. *Earth Planet. Sci. Lett.* **23**, 439–444 (1974).
34. A. Stettler, P. Eberhardt, J. Geiss, N. Grogler, S. Guggisberg, Chronology of the Apollo 17 Station 7 boulder and the south Serenitatis impact. *Proc. Lunar Planet. Sci. Conf.* **9**, 1113–1115 (1978).
35. G. Ryder, *Catalog of Apollo 17 Rocks. Volume 1: Stations 2 and 3 (South Massif)* (Johnson Space Center Curatorial Branch, Houston, TX, 1993).
36. T. Ishii, S. McCallum, S. Ghose, Petrological and thermal histories of a lunar breccia 73217 as inferred from pyroxene crystallization sequences, exsolution phenomena, and pyroxene geothermometry. *J. Geophys. Res.* **88**, A631–A644 (1983).
37. M. L. Crawford, Magma genesis by in situ melting within the lunar crust. *Proc. Lunar Planet. Sci. Conf.* **6**, 249–261 (1975).
38. H. Huber, P. H. Warren, Enigmatic, largely granitic 73217: A lunar mixed melt-breccia, but is it impact melt? *Proc. Lunar Planet. Sci. Conf.* **39**, 2405 (2008).
39. W. Compston, I. S. Williams, C. Meyer, U-Pb geochronology of zircons from lunar breccia 73217 using a sensitive high mass-resolution ion microprobe. *J. Geophys. Res.* **89**, B525–B534 (1984).
40. D. York, N. M. Evensen, M. L. Martínez, J. De Basabe Delgado, Unified equations for the slope, intercept, and standard errors of the best straight line. *Am. J. Phys.* **72**, 367–375 (2004).
41. R. K. Pearson, *Exploring Data in Engineering, the Sciences, and Medicine* (Oxford Univ. Press, New York, 2011).
42. G. B. Dalrymple, G. Ryder, ^{40}Ar/^{39}Ar age spectra of Apollo 15 impact melt rocks by laser step-heating and their bearing on the history of lunar basin formation. *J. Geophys. Res.* **98**, 13085–13095 (1993).
43. M. D. Norman, R. A. Duncan, J. J. Huard, Imbrium provenance for the Apollo 16 Descartes terrain: Argon ages and geochemistry of lunar breccias 67016 and 67455. *Geochim. Cosmochim. Acta* **74**, 763–783 (2010).
44. C. I. Fassett, D. A. Minton, Impact bombardment of the terrestrial planets and the early history of the Solar System. *Nat. Geosci.* **6**, 520–524 (2013).
45. F. J. Stadermann, E. Heusser, E. K. Jessberger, S. Lingner, D. Stöffler, The case for a younger Imbrium basin: New ^{40}Ar-^{39}Ar ages of Apollo 14 rocks. *Geochim. Cosmochim. Acta* **55**, 2339–2349 (1991).
46. D. Liu, B. L. Jolliff, R. A. Zeigler, R. L. Korotev, Y. Wan, H. Xie, Y. Zhang, C. Dong, W. Wang, Comparative zircon U–Pb geochronology of impact melt breccias from Apollo 12 and lunar meteorite SaU 169, and implications for the age of the Imbrium impact. *Earth Planet. Sci. Lett.* **319**, 277–286 (2012).
47. G. B. Dalrymple, G. Ryder, Argon-40/argon-39 age spectra of Apollo 17 highlands breccia samples by laser step heating and the age of the Serenitatis basin. *J. Geophys. Res.* **101**, 26069–26084 (1996).
48. M. Sharp, I. Gerasimenko, L. C. Loudin, J. Liu, O. B. James, I. S. Puchtel, R. J. Walker, Characterization of the dominant impactor signature for Apollo 17 impact melt rocks. *Geochim. Cosmochim. Acta* **131**, 62–80 (2014).
49. I. Wendt, C. Carl, The statistical distribution of the mean squared weighted deviation. *Chem. Geol.* **86**, 275–285 (1991).
50. F. Jourdan, C. Verati, G. Féraud, Intercalibration of the Hb3gr ^{40}Ar/^{39}Ar dating standard. *Chem. Geol.* **231**, 177–189 (2006).
51. B. D. Turrin, C. C. Swisher III, A. L. Deino, Mass discrimination monitoring and intercalibration of dual collectors in noble gas mass spectrometer systems. *Geochem. Geophys. Geosyst.* **11** (2010).
52. J. R. Wijbrans, I. McDougall, On the metamorphic history of an Archaean granitoid greenstone terrane, East Pilbara, Western Australia, using the ^{40}Ar/^{39}Ar age spectrum technique. *Earth Planet. Sci. Lett.* **84**, 226–242 (1987).
53. R. W. Stoenner, O. A. Schaeffer, S. Katcoff, Half-lives of argon-37, argon-39, and argon-42. *Science* **148**, 1325–1328 (1965).
54. R. Wieler, Cosmic-ray-produced noble gases in meteorites. *Rev. Mineral. Geochem.* **47**, 125–170 (2002).
55. A. O. Nier, A redetermination of the relative abundances of the isotopes of carbon, nitrogen, oxygen, argon, and potassium. *Phys. Rev.* **77**, 789 (1950).
56. R. H. Steiger, E. Jäger, Subcommission on geochronology: Convention on the use of decay constants in geo- and cosmochronology. *Earth Planet. Sci. Lett.* **36**, 359–362 (1977).
57. K. F. Kuiper, A. Deino, F. J. Hilgen, W. Krijgsman, P. R. Renne, J. R. Wijbrans, Synchronizing rock clocks of Earth history. *Science* **320**, 500–504 (2008).
58. P. R. Renne, K. Deckart, M. Ernesto, G. Feraud, E. M. Piccirillo, Age of the Ponta Grossa dike swarm (Brazil), and implications to Paraná flood volcanism. *Earth Planet. Sci. Lett.* **144**, 199–211 (1996).
59. P. R. Renne, C. C. Swisher, A. L. Deino, D. B. Karner, T. L. Owens, D. J. DePaolo, Intercalibration of standards, absolute ages and uncertainties in ^{40}Ar/^{39}Ar dating. *Chem. Geol.* **145**, 117–152 (1998).
60. A. Stettler, P. Eberhardt, J. Geiss, N. Grögler, P. Maurer, Ar^{39}-Ar^{40} ages and Ar^{37}-Ar^{38} exposure ages of lunar rocks. *Proc. Lunar Planet. Sci. Conf.* **4**, 1865–1888 (1973).
61. L. T. Aldrich, G. W. Wetherill, Geochronology by radioactive decay. *Annu. Rev. Nucl. Sci.* **8**, 257–298 (1958).
62. G. B. Dalrymple, Critical tables for conversion of K-Ar ages from old to new constants. *Geology* **7**, 558–560 (1979).

Acknowledgments: We thank H. Schmitt and G. Cernan for collecting the samples and returning them to Earth, where they continue to yield new scientific information more than four decades later. We also thank R. Zeigler, Apollo Sample Curator at NASA's Johnson Space Center, for supervising the expert preparation of new sections for this work. Earlier comments by F. Jourdan, C. Shearer, and others inspired us to refine our approach to presenting the data reported here, and we thank two anonymous reviewers for *Science Advances* for valuable comments on the final manuscript. **Funding:** This work was largely supported by NASA grant NNX11AB31G (with K.V.H. as the principal investigator and B.L.J. as the co-investigator) and a NASA Earth and Space Science Fellowship to C.M.M. (NNX12AH82H). **Author contributions:** J.R.W. and B.L.J. were primarily responsible for sample selection and characterization, with B.L.J. performing the petrographic analysis reported here. J.R.W., K.E.Y., and J.-A.W. prepared the samples for neutron irradiation. C.M.M. and K.E.Y. performed the laser microprobe analyses with assistance from J.-A.W. and M.C.v.S. C.M.M. was primarily responsible for data analysis and interpretation, with input from K.V.H. and J.-A.W. C.M.M. and K.V.H. wrote the paper, with input from all other authors.

Submitted 24 October 2014
Accepted 30 December 2014
Published 12 February 2015
10.1126/sciadv.1400050

Citation: C. M. Mercer *et al.*, Refining lunar impact chronology through high spatial resolution ^{40}Ar/^{39}Ar dating of impact melts. *Sci. Adv.* **1**, e1400050 (2015).